Int. J. Microgravity Sci. Appl., **35** (2) (2018) 350202
DOI: 10.15011//jasma.35.350202

IIII Original Paper IIII

Generation of a Large-Scale *n*-Decane-Droplet Cloud Considering Droplet Pre-Vaporization in "Group Combustion" Experiments aboard Kibo/ISS

Masato MIKAMI [1], Hiroshi NOMURA [2], Yusuke SUGANUMA [2],
Masao KIKUCHI [3], Takuma SUZUKI [3] and Masaki NOKURA [4]

Abstract

The first microgravity combustion experiments were carried out in 2017 aboard the Japanese Experiment Module "Kibo" on ISS, titled "Elucidation of Flame Spread and Group Combustion Excitation Mechanism of Randomly Distributed Droplet Clouds (Group Combustion)." The flame spread over a large-scale droplet cloud consisting of about 100 droplets randomly distributed on a SiC-fiber lattice was observed. When droplets are generated one by one, the diameter of a droplet generated earlier changes more during large-scale droplet-cloud generation. The droplet pre-vaporization effect needed to be well understood to generate large-scale droplet clouds with a uniform initial droplet diameter for "Group Combustion" experiments. We describe the concept of the large-scale droplet-cloud generation and report the vaporization-rate constants for a single droplet, for two interactive droplets and for a droplet cloud with *n*-decane as a fuel and verification results obtained in the "Group Combustion" experiments aboard ISS. The evaluation of the vaporization-rate constant during the droplet-cloud generation suggests that the droplet vaporization in the droplet cloud occurred with interaction among many more than three droplets. Considering the pre-vaporization with the vaporization-rate constant estimated, most droplets had a nearly uniform diameter at ignition. Satisfactory reproducibility was confirmed in the droplet diameter at ignition and the flame-spread behavior.

Keyword(s): Droplet vaporization, Droplet cloud, Combustion experiment, Space-based experiment, Kibo/ISS

Received 7 March 2018, accepted 17 April 2018, published 31 April 2018.

1. Introduction

Since Kumagai and Isoda [1] conducted the first microgravity experiments on single droplet combustion, many researches on the behavior of droplet combustion have been conducted in microgravity as fundamental researches for understanding spray combustion. Kumagai and Isoda [1] used a silica filament as the droplet holder. Kumagai et al. [2] realized the combustion of a free droplet in microgravity, by rapidly pulling out the silica-filament droplet suspender and igniting the free droplet by a spark. NASA developed a free-droplet generation method in which a liquid fuel is supplied between the tips of two stainless steel tubes and a free droplet is generated by rapidly retracting the two tubes in microgravity [3]. This method was employed in the single free-droplet combustion experiments in the Combustion Integrated Rack (CIR) aboard the International Space Station (ISS) [4]. The free-droplet combustion has the merit that there is no effect of the droplet holding fiber but has the demerit that it is too difficult to make it stationary in space even in microgravity. Due to this difficulty, there have been no combustion experiments using multiple free droplets.

Dietrich et al. [5] employed an SiC fiber whose diameter was one order smaller than the silica fiber of about 100 μm to tether the droplet. The droplet was generated on the fiber using a relatively large device, which was the same as the free-droplet generation device. Mikami et al. [6] discussed the effect of a 14 μm-SiC fiber on the shape and burning of a droplet of about 1-mm in diameter and concluded that it is negligible except for the later stage of combustion. They also developed a method of generating a droplet at the intersection of X-shaped 14-μm SiC fibers by supplying fuel using a glass-tube needle whose tip is narrowed to 40 μm. This method allows the droplet-generation device to be smaller and thus has been applied to experiments using multiple droplets. Microgravity experiments were

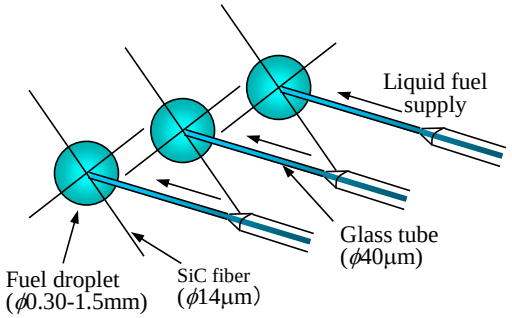

Fig. 1 Simultaneous multiple-droplet generation on X-shaped SiC fibers using fuel-supply glass-tube needles. [6]

1 Department of Mechanical Engineering, Yamaguchi University, 2-16-1 Tokiwadai, Ube, Yamaguchi 755-8611, Japan.
2 College of Industrial Technology, Nihon University, 1-2-1 Izumi-cho, Narashino, Chiba 275-8575, Japan.
3 JEM Utilization Center, Japan Aerospace Exploration Agency, 2-1-1 Sengen, Tsukuba, Ibaraki 305-8605, Japan.
4 IHI Inspection & Instrumentation Co., Ltd., 1-100 Takamatsu-cho, Tachikawa, Tokyo 190-0011, Japan.
(E-mail: mmikami@yamaguchi-u.ac.jp)

conducted on the flame spread of droplet arrays tethered on SiC fibers using a simultaneous multiple-droplet generation method with multiple fuel-supply glass-tube needles [6-8] as shown in **Fig. 1**. Furthermore, Mikami et al. [9] generated a droplet by a fuel-supply glass-tube needle at a designated position of an SiC-fiber lattice, repeated it by using a three-axis traverse system as shown in **Fig. 2** to form a droplet-cloud element consisting of four droplets and conducted the flame-spread experiment to study the flame-spread-limit distribution around two interactive droplets in microgravity.

This method was employed in the first microgravity combustion experiments carried out by our research group in 2017 aboard the Japanese Experiment Module "Kibo" on ISS, titled "Elucidation of Flame Spread and Group Combustion Excitation Mechanism of Randomly Distributed Droplet Clouds (Group Combustion)" [10]. Kikuchi et al. [11] reported the details of the Group Combustion Experiment Module (GCEM). The flame spread over a large-scale droplet cloud consisting of about 100 droplets randomly distributed on a SiC-fiber lattice was observed. This project studied local flame-spread characteristics and macroscopic flame-spread characteristics in order to improve the percolation model to describe the group-combustion excitation through the flame spread between droplets [12]. When droplets are generated one by one, the diameter of a droplet generated earlier changes more during large-scale droplet-cloud generation. Therefore, the droplet pre-vaporization effect needed to be well understood to generate large-scale droplet clouds with a uniform initial droplet diameter for "Group Combustion" experiments. In this paper, we describe the concept of large-scale droplet-cloud generation and report the verification results obtained in the "Group Combustion" experiments aboard ISS.

2. Droplet-cloud Generation Concept and Experimental Apparatus

2.1 Concept of a Large-scale Droplet-cloud Generation

First, we consider the droplet vaporization. The vaporization-rate constant of a droplet in the quasi-steady state is expressed as

$$K \equiv -\frac{d(d^2)}{dt} = 8D_G(\rho_G/\rho_L)\ln(1+B) \tag{1}$$

where d is the droplet diameter, D_G is the diffusion coefficient in the gas phase, ρ_G/ρ_L is the gas-liquid density ratio and B is the transfer number [13]. If the droplet vaporizes slowly like during the droplet generation process, the transfer number, B, is very small and thus Eq. 1 is approximated as

$$K = 8D_G(\rho_G/\rho_L)B. \tag{2}$$

B is expressed as

$$B = (Y_{f+} - Y_{fa})/(1 - Y_{f+}) \tag{3}$$

where Y_{f+} and Y_{fa} are the fuel mass fractions in the gas phase at the droplet surface and in the ambient gas, respectively. Therefore, the vaporization is driven by Y_{f+} and Y_{fa}.

Figure 3 shows a photograph of randomly distributed 97-*n*-decane droplets in GCEM aboard ISS. This photograph was taken at the hypothetical ignition time in the condition later shown in **Fig. 8**. It took longer than 20 minutes from the start of droplet generation of the first droplet till the completion of droplet generation of the last droplet in the droplet cloud. If the droplets

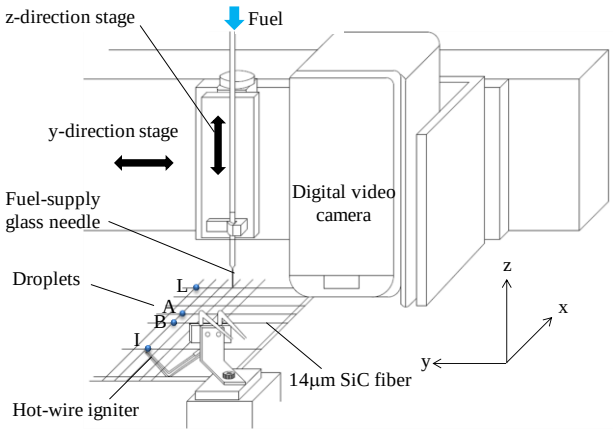

Fig. 2 Apparatus of droplet-cloud generation on an SiC-fiber lattice using a fuel-supply glass-tube needle and a three-axis traverse system. [9]

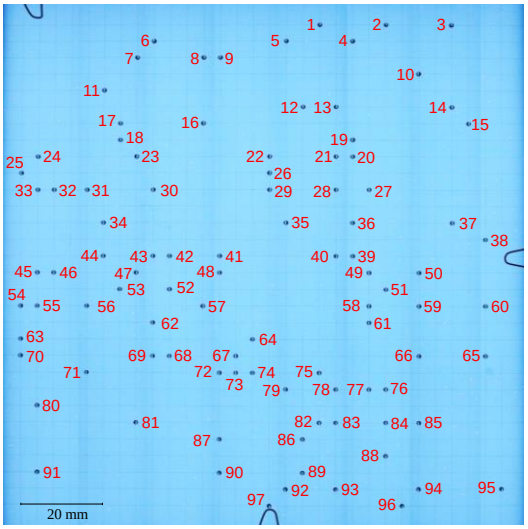

Fig. 3 Photograph of a randomly distributed *n*-decane-droplet cloud on a SiC-fiber lattice generated by GCEM in microgravity aboard Kibo/ISS. The droplet number for each droplet is also shown.

are generated one by one as explained in the Introduction, there are two methods to make all the droplets to have the same diameter at ignition as follows:

(A) Droplet generation in ambient gas with a saturated fuel vapor
(B) Droplet generation considering pre-vaporization of the droplets.

According to Eq. 3, the droplet does not vaporize if $Y_{fa}=Y_{f+}$, i.e., in ambient gas with a saturated fuel vapor. Therefore, Concept A generates a droplet cloud without the pre-vaporization effect. Here, the Clausius-Clapeyron relation shows the relation between the fuel mole fraction at the droplet surface in the gas phase, X_{f+}, and the droplet surface temperature, T, as

$$X_{f+} = exp\left[\frac{L}{R}\left(\frac{1}{T_b}-\frac{1}{T}\right)\right] \tag{4}$$

where L is the latent heat, R is the gas constant, and T_b is the boiling point at ambient pressure. X_{f+} is smaller at lower temperature, and thus Y_{f+} is smaller. In the case that there is a temperature distribution in the combustion chamber, even if the ambient gas contains fuel vapor saturated at a temperature near the droplet-cloud generation position, condensation occurs where the temperature is lower than the droplet-cloud generation position, and the fuel concentration becomes lower. Thus, slight vaporization would occur. Since GCEM was installed in the Chamber of Combustion Experiment (CCE) placed on a cold plate, the temperature of the bottom surface of the combustion chamber of GCEM is 0.5 K lower than that near the droplet-cloud generation position. Furthermore, a preliminary experiment in normal gravity revealed that some wire cover adsorbs fuel vapor and suppresses the saturated fuel vapor formation.

Next, in Concept B, in order to make the droplet diameter the same at the ignition timing, larger droplets are generated considering the diameter decrease of each droplet during the waiting time for ignition after each droplet generation. According to Eq. 1, the d^2-law

$$d_0^2 = d_{gi}^2 - K(t_0 - t_{gi}) \tag{5}$$

holds for the droplet diameter of the ith droplet d_{gi} at droplet generation time t_{gi} and the droplet diameter d_0 at ignition. Hence, a larger droplet needs to be generated if it is generated earlier. In order to estimate d_{gi} accurately, it is important to estimate the vaporization-rate constant K accurately. The "Group Combustion" experiments employed Method B. As explained in Section 3, K was experimentally obtained in long-duration microgravity aboard Kibo on ISS.

Lastly, we discuss the effect of pre-vaporization on the flame spread. As explained later, *n*-decane was used as the fuel and the temperature near the droplet cloud was maintained at 293 K. The equivalence ratio in the gas phase at the *n*-decane droplet surface is ϕ^+=0.09 at 293 K. Although the amount of pre-vaporization depends on the waiting time for ignition after the droplet generation, the maximum local equivalence ratio is ϕ^+, which is lower than the lower flammability limit. A premixed-flame cannot propagate in such a very lean mixture. If a diffusion flame exists in such a very lean mixture, part of the fuel vapor contributes to the reaction only through the diffusion process. Since ϕ^+=0.09 corresponds to the fuel mass fraction Y_F=0.0006, which is much smaller than the fuel mass fraction in the gas phase at the droplet surface $Y_F{}^+$=0.85 in the quasi-steady burning condition, the effect of pre-vaporization on droplet burning is negligible. Nomura et al. [14] conducted flame-spread experiments in fuel vapor/air mixtures in microgravity and reported that such a small equivalence ratio does not affect the flame spread significantly.

2.2 Experimental Apparatus and Procedures

The Group Combustion Experiment Module (GCEM) was used in this experiment. This subsection describes the experimental apparatus and procedures of GCEM in brief; details are reported in Ref. 11.

According to Concept B explained in Subsection 2.1, the droplet cloud was generated considering the droplet-diameter decrease due to pre-vaporization during the droplet-cloud generation process shown in Eq. 5. A 30×30 SiC-fiber lattice with 4-mm intervals of 14-μm SiC fiber (Nippon Carbon, Hi-Nicalon) was used to tether the droplets. *n*-Decane was supplied from a stepping-motor-driven syringe to the tip of the glass-tube needle through a Teflon tube with 1.67×10^{-3} mm^3/pulse, and a droplet was generated at a predetermined lattice point. The droplet diameter error caused by one stepping-motor-pulse error was 0.1 % for the droplet diameter at droplet generation d_g=1 mm. The position of the tip of the glass-tube needle was moved by a three-axis traverse system, and droplets were generated one by one to form a droplet cloud. As explained in the Introduction, the effect of the SiC fiber on the flame spread is negligible. The flame spread of the droplet cloud was started by the hot-wire ignition of a droplet on one side of the lattice. The droplet-cloud generation system and the ignition system were installed in a combustion chamber with an inner size of 282×235×205 mm.

A digital camera (Canon, EOS 5D Mark II) took still images of droplet clouds right after droplet generation and at the completion of the droplet-cloud generation and movies of the burning behavior through the glass window of the chamber. An LED back-light was used for the still images but was not used for the movie. Since the light-emitting area was 30×146 mm, the back-light did not cover the entire area of the droplet cloud. Thus, the back-light was traversed with the fuel-supply glass-tube needle while the still image was taken. The spatial resolutions of the still

image and the movie were 41.5 and 122 μm/pixel, respectively. The droplet diameter was measured from backlit still images based on the method described by Nomura et al.[14]. We detected the droplet surface every one pixel line, obtained the shape of droplet surface as an ellipse by the least square approximation and calculated an equivalent droplet diameter and position. Thus, the uncertainty of droplet diameter and position was 0.9 μm for 1 mm droplet.

GCEM was installed in CCE placed on a cold plate of the work volume of the Multi-purpose Small Payload Rack in Kibo. Thus the temperature near the droplet cloud was maintained at 293 K except during burning. A 21 vol% O_2/79 vol% N2 mixture was used as the ambient gas supplied from a gas bottle. The pressure inside the chamber was 101 kPa before ignition.

3. Results and Discussion

3.1 Vaporization of Single Droplet and Two Interactive Droplets

In order to estimate the vaporization-rate constant in microgravity, which is required for the large-scale droplet-cloud generation method, we conducted a preliminary experiment on the droplet vaporization of single *n*-decane droplet in normal gravity. **Figure 4** shows temporal variations of the droplet diameter squared at 301 K in normal gravity. For the Grashof number Gr<<1, the vaporization-rate constant in normal gravity, K_{1G}, is expressed as

$$K_{1G} = K_{0G}(1 + CGr^{1/2}) \quad (6)$$

where K_{0G} is the vaporization-rate constant in zero-gravity [15]. Since Gr is proportional to the third power of the droplet diameter, the instantaneous vaporization rate obtained from the slope of **Fig. 4** will approach K_{0G} as the droplet diameter, d, decreases to zero. The instantaneous vaporization rate approached about 0.0006 mm^2/s while d approached zero. The vaporization-rate constant at 293 K in zero-gravity is estimated as about 0.0004 mm^2/s considering the estimated one at 301 K, Eq. 4 and Eq. 3 with Y_{fa}=0.

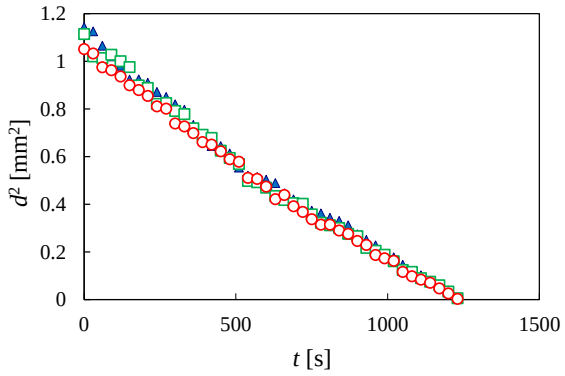

Fig. 4 Temporal variations of droplet dimeter squared during vaporization of single *n*-decane droplets for three different tests at 301 K in normal gravity.

Experiments on single and two interactive droplets were conducted using GCEM in long-duration microgravity aboard Kibo/ISS. As shown in **Fig. 3**, the local droplet spacing is not uniform in a randomly distributed droplet cloud. The vaporization-rate constant becomes smaller for smaller droplet spacing. **Figure 5** shows the *n*-decane droplet arrangement to study the vaporization-rate constants of two interactive droplets and single droplet at 293 K in GCEM, while the droplet spacing between two interactive droplets was 4 mm and the single droplet existed 44 mm away from the two interactive droplets. **Figure 6** shows d^2-t curves for three conditions with the single droplet. **Figure 7** shows d^2-t curves for one of three conditions with the two interactive droplets. **Table 1** shows the droplet diameter at droplet generation, d_g, the vaporization-rate constant obtained from the slope of the least-square-fitted line for each condition. As shown in **Figs. 6** and **7**, the vaporization time exceeded 50 minutes while the ambient temperature was maintained at 293 K. This is probably the first report on such a long-duration

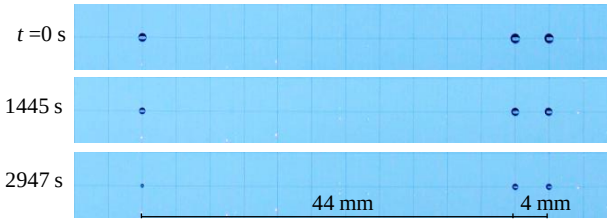

Fig. 5 Photographs of two interactive *n*-decane droplets with 4 mm droplet spacing and single *n*-decane droplet existed 44 mm away from the two interactive droplets at different elapsed times from droplet generation in microgravity.

Table 1 Droplet-vaporization-rate constants K for single and two droplets and interaction coefficient γ for two droplets at 293K in microgravity. Theoretical interaction coefficient by Eq. 8 is also listed.

d_g [mm]	K [mm^2/s]	S/d_g	γ	γ (Eq. 8)
0.973	0.000262	-	-	-
0.907	0.000265	-	-	-
0.771	0.000264	-	-	-
1.109	0.000245	3.6	0.93	0.803
1.101	0.000245		0.93	
0.858	0.000260	5	0.99	0.850
0.737	0.000251		0.95	
0.803	0.000254	5	0.97	0.851
0.779	0.000254		0.97	

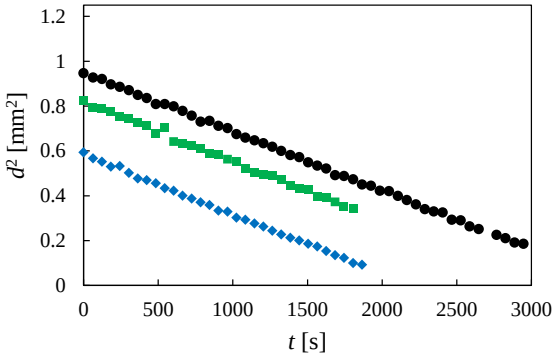

Fig. 6 Temporal variations of droplet dimeter squared during vaporization of single n-decane droplets for three different tests at 293 K in microgravity.

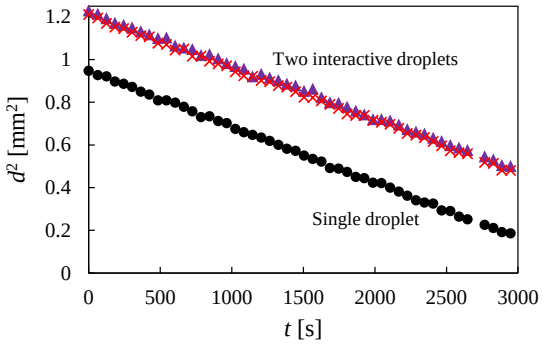

Fig. 7 Temporal variations of droplet dimeter squared during vaporization of two *n*-decane droplets with S/d_g=3.6 and a single droplet at 293 K in microgravity.

vaporization in microgravity. The average value of the vaporization-rate constants of the single droplet, K_S, shown in **Fig. 6** is K_S=0.00026 mm^2/s, which is smaller than the estimated value based on the preliminary experiment in normal gravity. As shown in **Table 1**, the vaporization-rate constant of each droplet in the two interactive droplets is somewhat smaller than K_S.

The interaction coefficient for two droplets, γ, which is the ratio of the vaporization-rate constant of two interactive droplets, K, to that of single droplet, K_S,

$$\gamma \equiv K/K_S, \tag{7}$$

is also listed in Table 1. The interaction coefficient was γ=0.93 for S/d_g=3.6 and γ=0.95-99 for S/d_g=5. Umemura et al. [16] theoretically obtained the interaction coefficient of two droplets based on steady-state analysis, which is expressed as

$$\gamma = 2\{(S/d)^2-1\}^{\frac{1}{2}}\sum_{n=0}^{\infty}\left[1 + \left[S/d+\{(S/d)^2-1\}^{\frac{1}{2}}\right]^{2n+1}\right]^{-1}. \tag{8}$$

This theoretical value is also listed in **Table 1**. The theoretical γ is smaller than the experimental γ. Although the dimensionless droplet spacing is S/d_g at droplet generation, the dimensionless droplet spacing, S/d, increases over time since the droplet diameter, d, decreases over time. The interactive effect between two droplets decreases and the instantaneous interaction coefficient increases over time. Therefore, the experimental γ expresses the average interaction state during the vaporization and is greater than the theoretical γ in the steady-state with S/d_g.

3.2 Generation of a Large-scale Droplet Cloud

Next, a randomly distributed droplet cloud with 97 droplets was generated, and the droplet diameters at the ignition timing were examined. The diameter of the ith droplet at droplet generation, d_{gi}, was set as

$$d_{gi}^2 = d_0^2 + K(t_0 - t_{gi}) \tag{9}$$

for d_0=1mm. At first, K_S was used as K. Even if the interactive effect between two droplets shown in Eq. 8 is considered in K in Eq. 9, the droplet diameter at ignition is estimated to be about 1% different from that without considering the interactive effect. Since the droplet-generation error is greater than this difference, we used K_S as K in Eq. 9 for all droplets at first.

Figure 8 shows the droplet diameter at droplet generation, d_g, and the droplet diameter at the ignition timing, d_0, for each droplet number. d_g is the droplet diameter right after the completion of each droplet generation and was measured using a photograph taken during the droplet-cloud generation process with a back-light. Such photographs were not taken for all droplets by the present system. As shown in **Fig. 8**, the droplet diameter at the ignition timing, d_0, was on the whole greater than the target diameter of 1 mm although the diameter of the droplet generated

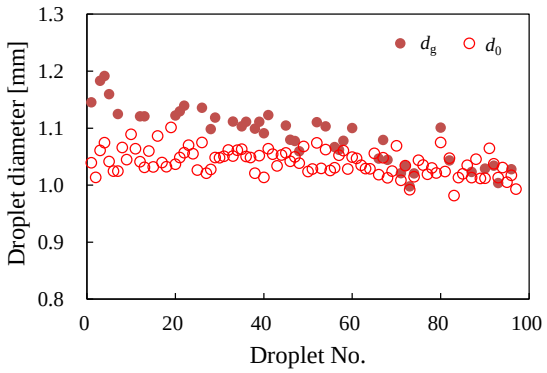

Fig. 8 Droplet diameters at droplet generation, d_g, and at ignition, d_0, in the case of droplet generation without considering droplet interaction in microgravity.

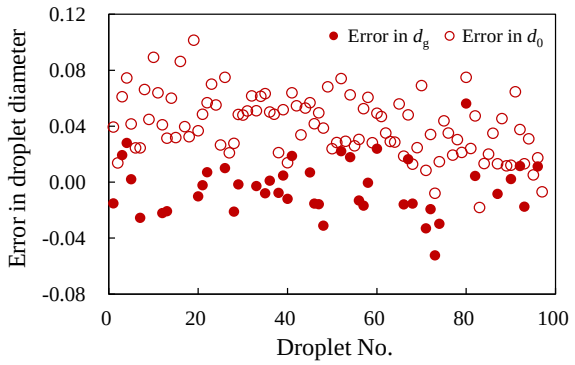

Fig. 9 Deviations of droplet diameters at droplet generation, d_g, and at ignition, d_0, from each target diameter in microgravity.

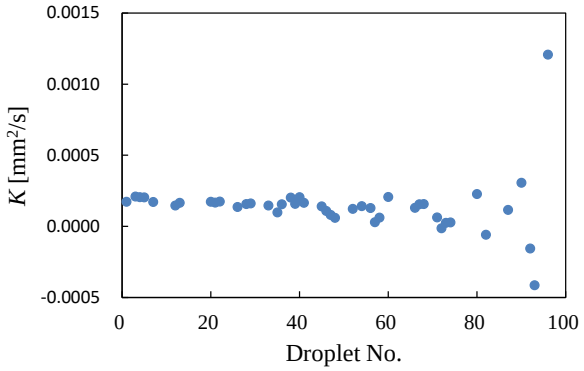

Fig. 10 Vaporization-rate constant during the droplet-cloud generation process in microgravity.

earlier seems to decrease more. **Figure 9** shows the errors in d_g and d_0. Although there was a case with 5.6% error in d_g, the error in d_g was less than 3% in most droplets. The error in d_0, however, deviated in the positive direction and seems greater for a smaller droplet number. This suggests that the vaporization-rate constant for the droplet cloud was smaller than that of single droplet, K_S.

Figure 10 shows the vaporization-rate constant for each droplet obtained based on the difference in the droplet diameter squared between the droplet generation timing of each droplet and the ignition timing. The vaporization-rate constant was smaller than K_S=0.00026 mm^2/s except for that of Droplets 90 and 96 while the error in the estimation of the vaporization-rate constant becomes greater for the larger number droplet, which had a shorter waiting time for ignition after droplet generation. Since the ambient temperature during the droplet-cloud generation was maintained at 293 K, the smaller vaporization-rate constant was due to the droplet interaction.

The interaction coefficient, γ, obtained from **Fig. 10** is plotted against the droplet spacing S/d_g between the nearest droplet pair for Droplets 1-46 in **Fig. 11**. Here, d_g is the average droplet diameters of the droplet pair at droplet generation. If a pairing droplet was not photographed, the diameter of the pairing droplet

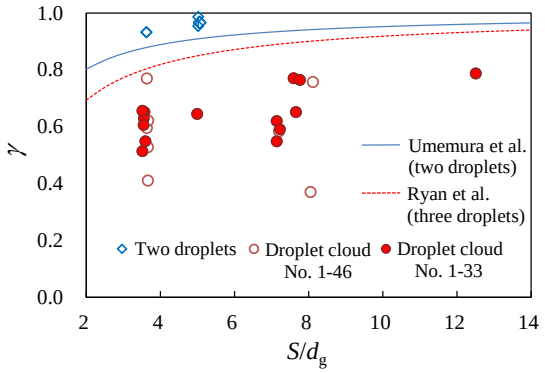

Fig. 11 Interaction coefficient γ vs. local droplet spacing at droplet generation, S/d_g, for two droplets and that for a randomly distributed droplet cloud in microgravity. Theoretical interaction coefficients of two droplets [16] and three droplets [17] in steady state are also shown.

was estimated using the droplet diameters of the two nearest droplets that were photographed. **Figure 11** shows the theoretical interaction coefficient of two droplets by Umemura et al. [16] (Eq. 8) and that of three droplets by Ryan et al. [17] expressed as

$$\gamma = \{1 + 0.882(S/d)^{-1}\}^{-1}. \tag{10}$$

Although the results for Droplets 1-33 suggest that γ was smaller for smaller S/d_g, the results for Droplets 1-46 suggest that the scatter of γ was within experimental error. Anyway, γ was smaller than that for the three-droplet interaction. Therefore, the droplet vaporization in the randomly distributed droplet cloud is not determined by the local droplet spacing between the nearest droplet pair but is affected by the interaction among many more than three droplets.

Next, we obtain the vaporization-rate constant by assuming that all droplets had the same vaporization-rate constant in the droplet cloud. If the droplet-diameter deviation, α_i, of ith droplet at ignition from the target diameter of 1 mm was due to the lowered vaporization rate alone, the equation below holds,

$$\{d_0(1 + \alpha_i)\}^2 = d_{gi}^2 - \gamma K_S(t_0 - t_{gi}), \tag{11}$$

where the droplet generation error is not considered. As explained above, the d_{gi} was set for d_0=1 mm as

$$d_{gi}^2 = d_0^2 + K_S(t_0 - t_{gi}). \tag{12}$$

Equations 11 and 12 give α_i as

$$\alpha_i = (1 - \gamma)K_S(t_0 - t_{gi})/(2d_0^2). \tag{13}$$

α_i is plotted against the vaporization time, t_0-t_{gi}, for each droplet in **Fig. 12**. The slope of the least-square fitted line of **Fig. 12** gives the vaporization-rate constant K=0.00017 mm^2/s and the

interaction coefficient γ=0.65. A modified error of the droplet diameter at ignition by subtracting the off-set due to the lowered vaporization rate is plotted against the error of droplet diameter at droplet generation in **Fig. 13**. This graph suggests that if the droplet cloud is generated considering an appropriate vaporization-rate constant, the error of the droplet diameter at ignition can be less than 5% even if there is an error in the droplet diameter at droplet generation.

3.3 Reproducibility of Droplet-cloud Generation and Flame Spread

97-droplets with the same droplet arrangement as in **Fig. 3** were generated twice with γ=0.7 considering the uncertainty in obtaining γ from **Fig. 12**, and the flame-spread experiment was conducted twice.

The droplet diameter at ignition d_0, i.e., the initial droplet diameter, is plotted against the droplet number for two experiments in **Fig. 14**. Although there were some droplets with large deviation in d_0, the initial droplet diameter existed overall within a certain range. The mean droplet diameter and the relative standard deviation were respectively 1.03mm and 2.4% in the first experiment and 1.05 mm and 4.5% in the second experiment. We can say that the reproducibility in the initial droplet diameter was satisfactory. One of the reasons why the mean initial droplet diameter was greater than 1 mm might be that we set a greater γ (=0.7) than that obtained from **Fig. 12**. Great deviations were found in Droplet 47 for the first experiment and Droplets 74 and 88 for the second experiment. The reason for it has not been elucidated.

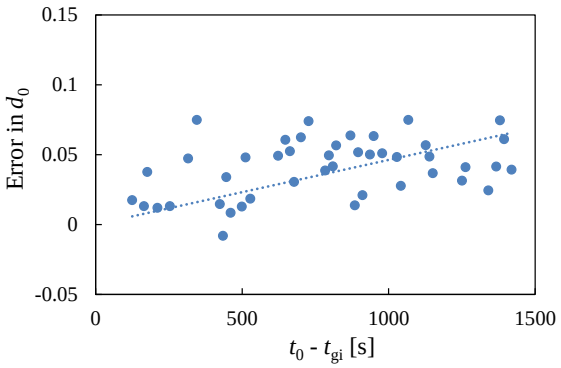

Fig. 12 Deviations of the droplet diameter at ignition, d_0, from the target diameter vs. waiting time for ignition after droplet generation in microgravity.

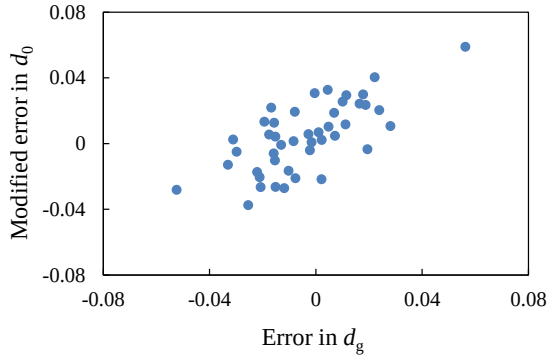

Fig. 13 Modified deviation of the droplet diameter at ignition, d_0, vs. deviation of the droplet diameter at droplet generation, d_g, in microgravity.

Figure 15 displays sequential photographs of the flame spread over 97-droplet clouds for the two experiments. In the first experiment shown in **Fig. 15a**, we employed a camera setting with the automatic exposure. In the second experiment shown in **Fig. 15b**, we employed another camera setting for the thin-filament pyrometry (TFP) to obtain the temperature from the light emission of SiC fibers with the exposure time of 1/60 s, F6.3 and ISO1250. The brightness of the photographs shown in **Fig. 15b** was enhanced by 80% from the original images. The elapsed time t from ignition is normalized by d_0^2, which is the square of the mean initial droplet diameter of the droplet cloud. The flame spread started from a small spherical flame around a single fuel droplet at t/d_0^2=0 and then spread across the droplet cloud until finally, a large-scale group flame appeared. The flame first reached a droplet on the top side of the lattice at t/d_0^2=4.25 s/mm^2 in **Fig. 15a** and t/d_0^2=4.13 s/mm^2 in **Fig. 15b**. Since the time difference for the same-phase flame-spread behavior occurrence was equal to or less than 3%, the reproducibility in the flame-spread behavior was considered satisfactory. One apparent different point is that the flame spread to Droplet 95 in the lower right area at t/d_0^2=3.37 s/mm^2 in **Fig. 15b** but did not spread to it in **Fig. 15a**. Droplet 95 conceivably exists near the flame-spread limit, where the flame spread is sensitive to a smaller difference in the initial condition. The details in the local flame-spread behavior will be reported in the next paper.

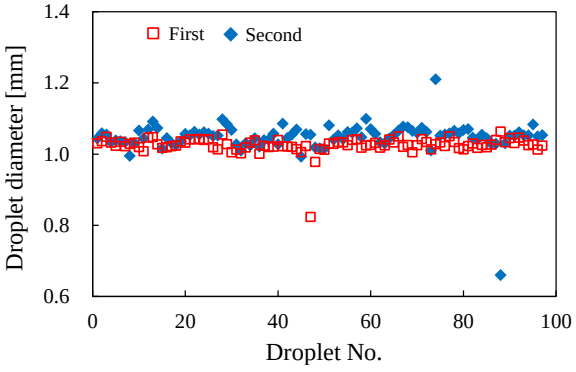

Fig. 14 Reproducibility in the droplet diameter at ignition in microgravity.

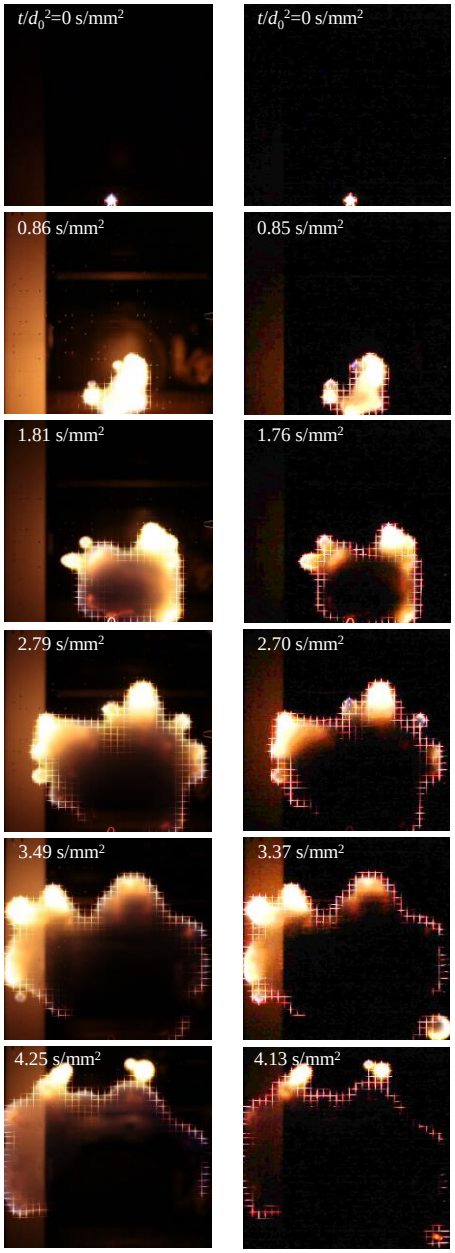

(a) First experiment (b) Second experiment

Fig. 15 Reproducibility in the flame-spread behavior over randomly-distributed droplet cloud in microgravity.

4. Concluding Remarks

This research generated large-scale droplet clouds in long-duration microgravity aboard Kibo/ISS and conducted experiments on the flame spread over randomly distributed 97-*n*-decane droplets for the first time.

We employed a large-scale droplet-cloud generation method considering the pre-vaporization of *n*-decane droplets during the droplet-cloud generation process. As fundamental vaporization data, we obtained the vaporization-rate constants for a single droplet and for the two interactive droplets at 293 K in microgravity by observing the droplet vaporization over 50 minutes. We also reconfirmed that the droplet interaction makes the vaporization-rate constant smaller. The evaluation of the vaporization-rate constant during the droplet-cloud generation revealed that the vaporization-rate constant in the droplet cloud was smaller than that for two droplets and the theoretical value for three droplets in the steady state, suggesting that the droplet vaporization in the droplet cloud occurred with interaction among many more than three droplets. Considering the pre-vaporization with the vaporization-rate constant estimated, most droplets had a nearly uniform diameter at ignition. Satisfactory reproducibility was confirmed in the droplet diameter at ignition and the flame-spread behavior.

The local flame-spread behavior will be reported in detail in the next paper.

Acknowledgements

This research was conducted as Kibo utilization experiments called “Group Combustion” by JAXA. We wish to thank Mr. S. Hiraga for his help in the droplet analysis.

References

1) S. Kumagai and H. Isoda: Symp. (Int.) Combust., **6** (1957) 726.
2) S. Kumagai, T. Sakai and S. Okajima: Symp. (Int.) Combust., **13** (1971) 779.
3) J.B. Haggard Jr. and J.L. Kropp: AIAA Paper, **87**-0576 (1987).
4) D.L. Dietrich, V. Nayagam, M.C. Hicks, P.V. Ferkul, F.L. Dryer, T. Farouk, B.D. Shaw, H.K. Suh, M. Y. Choi, Y.C. Liu, C.T. Avedisian and F. A. Williams: Microgravity Sci. Technol., **26** (2014) 65.
5) D.L. Dietrich and J.B. Haggard Jr.: Second International Microgravity Combustion Workshop, (1993) 317.
6) M. Mikami, H. Oyagi, N. Kojima, Y. Wakashima, M. Kikuchi and S. Yoda: Combust. Flame, **141** (2005) 241.
7) M. Mikami, H. Oyagi, N. Kojima, Y. Wakashima, M. Kikuchi and S. Yoda: Combust. Flame, **146** (2006) 391.
8) H. Oyagi, H. Shigeno, M. Mikami and N. Kojima: Combust. Flame, **156** (2009) 763.
9) M. Mikami, H. Watari, T. Hirose, T. Seo, H. Saputro, O. Moriue and M. Kikuchi: J. Thermal Sci. Technol., **12** (2017) JTST0028.
10) M. Mikami, M. Kikuchi, Y. Kan, T. Seo, H. Nomura, Y. Suganuma, O. Moriue and D.L. Dietrich: Int. J. Microgravity Sci. Appl., **33** (2016) 330208.
11) M. Kikuchi, Y. Kan, A. Tazaki, S. Yamamoto, M. Nokura, N. Hanafusa, Y. Hisashi, O. Moriue, H. Nomura and M. Mikami: Trans. JSASS Aerospace Tech. Japan, **12** (2014) No. ists29, Th_25-Th_30.
12) M. Mikami, H. Saputro, T. Seo and H. Oyagi: Microgravity Sci. Technol., (2018) in press, DOI: 10.1007/s12217-018-9603-z.
13) F.A. Williams, Combustion Theory (2nd Ed.), Chapter 3, Benjamin/Cummings, Menlo Park CA (1985).
14) H. Nomura, H. Takahashi, Y. Suganuma and M. Kikuchi: Proc. Combust. Inst., **34** (2013) 1593.
15) J. Sato, M. Tsue, M. Niwa and M. Kono: Combust. Flame, **82** (1990) 142.
16) A. Umemura, S. Ogawa and N. Oshima: Combust. Flame, **41** (1981) 44.
17) W. Ryan, K. Annamalai and J. Caton: Combust. Flame, **80** (1990) 313.